Giant deformations and soft-inflation in LCE balloons

Andrea Giudici[1] and John S. Biggins[1]

Department of Engineering, University of Cambridge, Trumpington St., Cambridge CB21PZ, U.K.

Abstract – We propose that ballooning can be controlled, enriched and amplified by using rubbery networks of aligned molecular rods known as liquid crystal elastomers (LCEs). Firstly, LCEs are promising artificial muscles, showing large spontaneous deformations in response to heat and light. In LCE balloons, spontaneous deformations can trigger classic ballooning, either as phase-separation (at constant volume) or a volume jump (at constant pressure), resulting in greatly magnified actuation strains. Secondly, even at constant temperature, LCEs have unusual mechanics augmented by soft-modes of deformation in which the nematic director rotates within the elastomer. These soft modes enrich the mechanics of LCE balloons, which can also "balloon" between rotated and unrotated states, either during the classic instability, or as a separate pre-cursor, leading to successive instabilities during inflation.

Introduction. – Cylindrical balloons, commonly encountered at parties, have N shaped pressure-volume curves, where the negative gradient generates classic ballooning instabilities during inflation [1]. Under pressure control, the balloon jumps in volume at the pressure maximum, to a substantially larger (ballooned) state. Under volume control, the cylinder instead phase-separates into ballooned and un-ballooned portions [2–4]. Here, we show this instability can be controlled, enriched and amplified in balloons made from liquid crystal elastomers (LCEs).

LCEs [5] are rubbery networks of rod-shaped mesogens. Like conventional liquid crystals [6], the rods show a phase transition from an isotropic orientation distribution to an aligned nematic phase upon cooling through a critical temperature. In elastomers, alignment causes a dramatic reversible elongation along the (unit) director $\boldsymbol{n}$, (Fig. 1 (a)i), making LCEs soft actuators [7,8]. However, macroscopic actuation requires monodomain alignment. Experimentally, this is achieved by imprinting a preferred director during fabrication, commonly by cross-linking under stress [7] or in a monodomain nematic state [9], and imprinting inevitably renders the alignment transition (and actuation) super-critical. LCE bubbles/balloons have been fabricated [10,11] but their instabilities remain unexplored. Here, we show that LCE thermal actuation can trigger the ballooning instability (Fig. 1(a)ii), transforming LCEs into sub-critical actuators with greatly amplified strain.

LCEs also have very unusual mechanics in the nematic state, stemming from director rotation within the elastomer. In an (idealised) perfectly-isotropic monodomain LCE, any director could be chosen on cooling, leading to a degenerate set of ground-states connected by perfectly soft Goldstone-deformations [12,13]. For example, stretch perpendicular to $\boldsymbol{n}$ (Fig. 1(b)) could be accommodated at

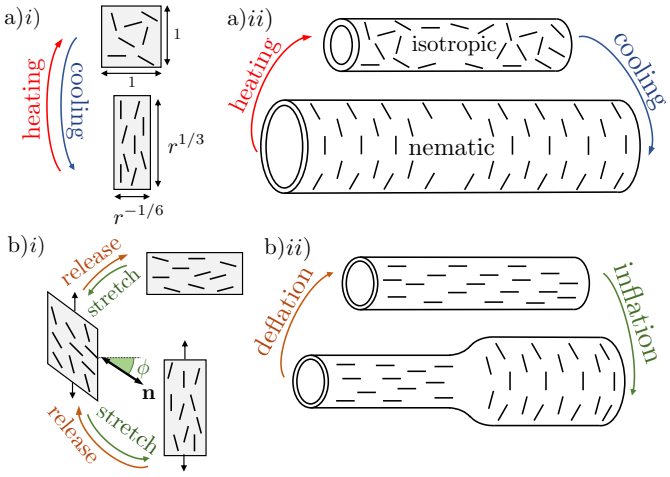

Fig. 1: Top: A monodomain LCE strip elongate on cooling from isotropic to nematic. In an LCE balloon cooled at constant pressure, this triggers a giant sub-critical volume jump. Bottom: Under stretching an LCE strip can director-rotate, softening the response. Under inflation, reorientation can become sub-critical, leading to phase separation between rotated and un-rotated segments. In both cases, the ballooned state has large radial and longitudinal stretches, limited only by finite extensibility of the LCE.

zero stress entirely by director rotation. Real monodomain LCEs show very similar behaviour, although the imprinted preferred director breaks the perfect degeneracy, so ideally soft deformations actually require a modest stress [14,15]. Here, We also consider the inflation of an aligned LCE balloon. During inflation, there is both longitudinal and azimuthal tension, so these deformations differ from those in strips under uniaxial tension (Fig. 1(b)i). However, we find that director rotation is nevertheless induced towards the dominating azimuthal stress (due to the cylindrical shape) leading to ballooning between fully-rotated and unrotated states (Fig. 1(b)). This may entirely precede the classical ballooning, leading to a balloon with consecutive instabilities during inflation.

Classical Ballooning. – We first consider a cylindrical rubber balloon, inflated to a desired volume strain $v = V/V_0$. The balloon instability can be traced to the elastic energy $w(v)$. As shown in Fig. 2a), if $w(v)$ has a concave region, $v^- < v < v^+$, and the balloon is inflated into this region, it is advantageous to phase separate (at fixed enclosed volume) into length-fractions at v_a and v_b, as the connecting chord lies below $w(v)$. Optimal separation is achieved by the common tangent construction:

$$w'(v_a) = w'(v_b), \qquad w(v_b) = w(v_a) + w'(v_a)(v_b - v_a).$$

As shown in Fig. 2b), concavity in $w(v)$ endows the pressure curve, $p \equiv \partial w/\partial V = (1/V_0)w'(v)$, with an unstable negative-gradient, leading to the characteristic N shape. Upon passing v^-, the balloon phase separates and drops to the Maxwell coexistence-pressure $p_M = p(v_a) = p(v_b)$, which can be found via common-tangents, or the equal area rule for A and B. Further inflation is accommodated by enlarging the length-fraction of v_a [2], moving along the energy chord at p_M. Phase separation ends at v_b, while in deflation it starts at v^+ and ends at v_a.

However, if the balloon is inflated using a pressure-controlled pump, the form of the instability is quite different. The balloon will dilate homogeneously to v^-, and then jump to a fully ballooned state at the same pressure. In deflation, un-ballooning occurs with a jump from v^+.

Convexity in $w(v)$ stems from the geometry of large strains. Consider inflating a capped cylindrical membrane so that its length increases $L \to \lambda L$, its radius increases, $R \to \eta R$, and, since the rubber is incompressible, membrane thickness decreases, $H \to H/(\eta\lambda)$. In cylindrically-oriented locally-Cartesian coordinates $(\hat{\boldsymbol{z}}, \hat{\boldsymbol{\theta}}, \hat{\boldsymbol{\rho}})$, the membrane's deformation gradient is $\mathbf{F} = \mathrm{diag}(\lambda, \eta, 1/(\eta\lambda))$, and the enclosed volume increases from $V_0 = \pi R^2 L$ to $V = \pi(\eta R)^2 \lambda L$: a volume strain $v \equiv V/V_0 = \eta^2\lambda$.

The simplest model of rubber elasticity treats its polymers as infinitely-extensible Gaussian chains [16], leading to the neo-Hookean energy density, $W(\boldsymbol{F}) = \frac{1}{2}\mu I_1$, where $I_1 = \mathrm{Tr}(\mathbf{F}^T \cdot \mathbf{F})$ is the first invariant of right Cauchy-Green tensor $\mathbf{F}^T \cdot \mathbf{F}$, and evaluates to the square-sum of the principle stretches. A neo-Hookean balloon with shear

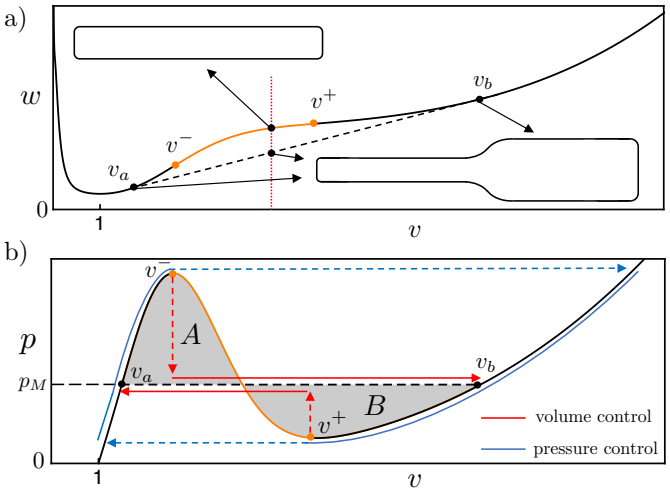

Fig. 2: (a) Energy and (b) pressure as a function of volume strain v of a conventional rubber cylindrical balloon. Energy concavity (orange) generates an N shaped pressure. Hysteresis loops of volume and pressure control are shown in red and blue.

modulus μ and (fixed) volume of rubber $2\pi RHL$ thus stores energy

$$w_0 = \mu\pi RHL\left(\eta^{-2}\lambda^{-2} + \eta^2 + \lambda^2\right). \tag{1}$$

However, during inflation, we do not control η and λ, but the inflationary volume strain v. We thus substitute $\lambda = v/\eta^2$ and set η to its minimising value ($\eta_{min} = (2v^4/(v^2+1))^{1/6}$) to obtain energy and pressure as a functions of v:

$$w_0(v) = 3\mu\pi RHL\left(\tfrac{1}{2}v + \tfrac{1}{2}v^{-1}\right)^{2/3} \tag{2}$$

$$p_0(v) = (\mu H/R)\left(\tfrac{1}{2}v + \tfrac{1}{2}v^{-1}\right)^{-1/3}\left(1 - v^{-2}\right). \tag{3}$$

We now see the cause of ballooning: $w_0(v)$ is concave beyond $v_0^- \equiv \sqrt{4+\sqrt{21}}$, [17], giving a pressure maximum $p_0^- = 0.749...\mu H/R$. Ballooning is indeed geometric: at large v, membrane strains scale as $v^{1/3}$, giving a concave energy $\propto v^{2/3}$. This simple model captures ballooning's onset, but $w_0(v)$ does not regain convexity at high v, so v_b is divergent. To correct this, we must account for finite chain extensibility, which impose a finite extensibility on the rubber. This is best done using the Gent energy [18],

$$W_G(I_1) = -J_m \log\left(1 - (I_1 - 3)/J_m\right), \tag{4}$$

where J_m is a phenomenological limiting value of the strain measure $I_1 - 3$. Up to an additive constant, Gent matches neo-Hookean for small strains, $(I_1 - 3 \ll J_m)$ but it always regains convexity [3,4], suggesting that the amplitude of v_b is limited by the finite chains. Unfortunately with Gent, analytic results for $v^\pm$, p_M, v_a and v_b are not available. However, in a typical rubber balloon, $J_m \sim 80$ is very large, so the onset of instability at v^- is well described by neo-Hookean. In most of what follows, we will thus restrict attention to neo-Hookeans, with the implicit assumption that convexity is regained at high v. However,

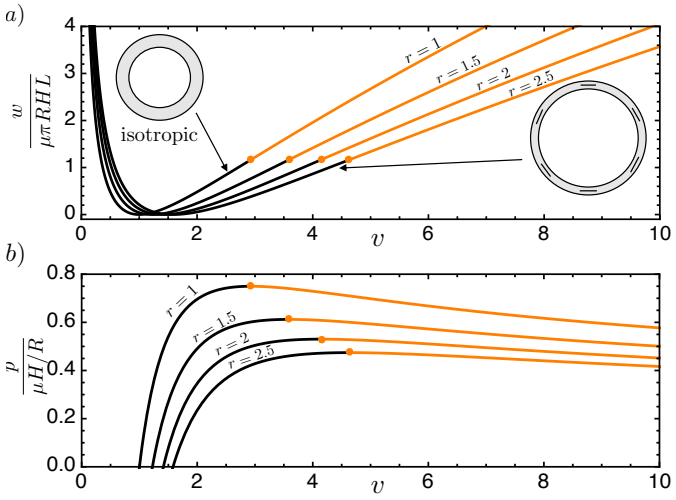

Fig. 3: Evolution of neo-Hookean energy and pressure curves for a cylindrical LCE balloon as it is actuated from isotropic ($r = 1$) to nematic ($r > 1$). Volume strain, v, is with respect to the isotropic state. The concave region in the energy, corresponding to a negative gradient in the pressure, is highlighted in orange.

since both energies depend on $\boldsymbol{F}$ only via I_1, the same (local) deformations always minimise both energies (e.g. same η_{min}), so one may compute Gent energy/pressure curves by substituting neo-Hookean fields into W_G.

Nematic-Isotropic Ballooning. – We now consider an LCE balloon, prepared with an azimuthal director, as shown in Fig. 1a. This monodomain balloon could be prepared Finkelmann-style [7] by cross-linking under inflation [10,11] (so the dominating azimuthal hoop stress imprints azimuthal alignment) or by rolling a planar monodomain.

For simplicity, we take the isotropic state of the balloon as the elastic reference state, with length L, radius R and thickness H. While isotropic, the LCE behaves just like a conventional rubber, with energy $w_0(v)$ and pressure $p_0(v)$ as above. However, on cooling, the rods align and bias the polymer configurations into prolate forms extended along $\boldsymbol{n} = \hat{\boldsymbol{\theta}}$. Microscopically, these chains are described by a prolate "step-length-tensor" which describes the bias of their random walks [5]:

$$\boldsymbol{l} = r^{-1/3}\left(\boldsymbol{\delta} + (r-1)\boldsymbol{nn}\right). \tag{5}$$

The phenomenological chain anisotropy parameter r subsumes the degree of nematic order and nematic-polymer coupling, while the pre-factor $r^{-1/3}$ ensures $\mathrm{Det}(\boldsymbol{l}) = 1$. A natural generalisation of the neo-Hookean stat-mech argument then leads to the LCE energy density [5]

$$W(F) = \tfrac{1}{2}\mu \mathrm{Tr}(\boldsymbol{F}^T.\boldsymbol{l}^{-1}.\boldsymbol{F}). \tag{6}$$

When the LCE is isotropic, we have $r = 1$ and $\boldsymbol{l} = \boldsymbol{\delta}$: standard neo-Hookean. However, on cooling, r grows above one. As illustrated in Fig. 1(a)i, the energy is then minimised by the spontaneous deformation $\boldsymbol{F_s} = \boldsymbol{l}^{1/2} = \mathrm{diag}\left(r^{-1/6}, r^{1/3}, r^{-1/6}\right)$, i.e. an elongation by $r^{1/3}$ along $\mathbf{n}$. In principle, r is also a function of stress, but for simplicity we neglect this effect. Stress induced changes to the nematic order parameter were indeed very modest in the original Finkelmann LCEs [5,19], but we note that other types of LCEs have recently shown substantial stress induced changes to the order parameter [11,20], and would correspondingly require a more sophisticated treatment. The energy has a multiplicative-decomposition structure, familiar from elastic models of growing tissues [21]. Accordingly, if we substitute $\boldsymbol{F} = \boldsymbol{F_2}\cdot\boldsymbol{F_s}$ (and fix $\boldsymbol{n} = \hat{\boldsymbol{\theta}}$) we recover the original neo-Hookean energy, but for deformations $\boldsymbol{F_2}$ from the spontaneously distorted state.

If the balloon were cooled at zero pressure, the spontaneous distortion would cause it to adopt a new relaxed shape with dilated radius, $R \to r^{1/3}R$, diminished length $L \to r^{-1/6}L$ and diminished thickness $H \to r^{-1/6}H$: a spontaneous volume strain $v_s = \sqrt{r}$. As above, we decompose the volume strain as $v = v_2 v_s$, with v_2 being the strain from this relaxed state. On inflation, the energy is thus simply $w_0(v_2)$, which, in terms of v, gives:

$$w_s(v) = w_0\left(v/\sqrt{r}\right), \quad p_s(v) = p_0(v/\sqrt{r})/\sqrt{r}. \tag{7}$$

As the balloon cools, the energy minimum moves to $v = v_s = \sqrt{r}$, and the instability threshold similarly moves to $v^- = v_0^- v_s$ (Fig 3a). These are geometric consequences of the larger relaxed volume. The pressure curves, Fig 3b, similarly dilate along the v axis by $\sqrt{r}$, but also diminish in height by $\sqrt{r}$ due to the reduced relaxed thickness.

These observations lead to two possibilities for temperature controlled ballooning. If we heat at fixed volume the leftward shift of the instability point will cause the balloon to suddenly phase-separate when $v = v_0^-\sqrt{r}$. This possibility is shown as the red isochor on Fig. 4, where we now deploy Gent pressure curves predicting finite amplitude. Conversely, if we cool at constant pressure, (blue isobar) the diminishing height of the $p - v$ curve can cause the LCE to jump to a fully ballooned state when $p = p_0^-/\sqrt{r}$.

In both cases, the LCE actuation is transformed. To create an actuating mono-domain, one must imprint a preferred director through the elastomer, either by stretching during cross-linking [7] or by cross-linking in an aligned liquid nematic state [22,23]. Imprinting renders monodomain LCEs supercritical, with continuous actuation over a considerable temperature range [5]. However, ballooning transforms LCEs into sub-critical actuators: the strain in the LCE jumps as the ballooning threshold is passed. Furthermore, the strain in the ballooned state is $v_b \sim J_m^{3/2}$, reflecting the finite extensibility of the polymer chains, and far larger than the LCE's intrinsic actuation strain. A similar principle has been deployed to amplify voltage driven actuation in dielectric elastomer balloons [24,25]. Such deformations may be termed giant, as their limiting value reflects different physics to their origin.

A simpler experimental option may be to take an LCE balloon crosslinked in the high-T isotropic state without

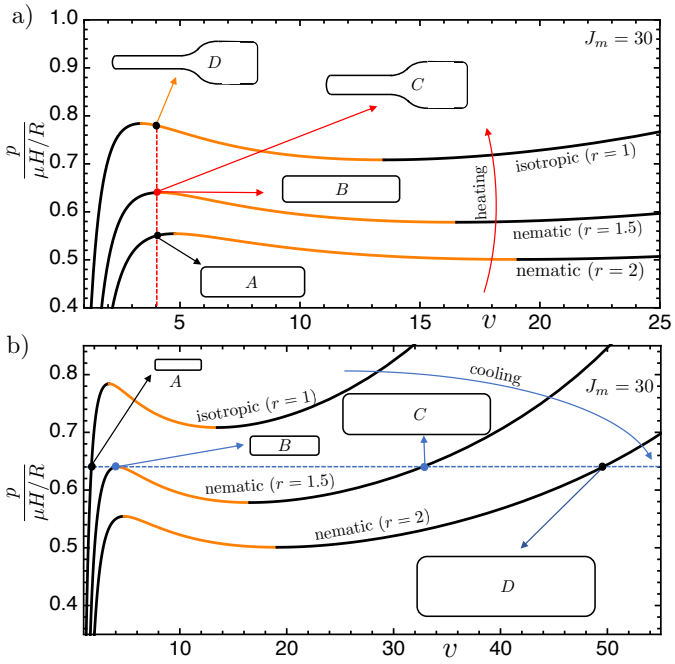

Fig. 4: Gent pressure curves for an LCE balloon when isotropic ($r = 1$) and nematic ($r = 1.5$ and $r = 2$). In each figure we also show the evolution of balloon shape, $A \to B \to C \to D$ during (a) heating at constant volume and (b) cooling at constant pressure. In (a), as the pressure maximum (instability point) traverses the imposed volume (dashed red line), the balloon suddenly phase separates, $B \to C$. In (b), as the pressure maximum traverses the imposed pressure (dashed blue line) a giant sub-critical volume jump is triggered, $B \to C$.

imprinting $\boldsymbol{n}_0$. The nematic-isotropic transition is now first order, reflecting the non-polar nature of the nematic phase [6]. On cooling, such LCEs form 'isotropic-genesis' polydomains, without macroscopic actuation. However, such samples are "super-soft" [26, 27] with even a very slight stress being sufficient to align the director and deliver the monodomain deformation $\sim r^{1/3}$. In a pressurised balloon, the dominating azimuthal stress would guide the director azimuthally on cooling, leading to above actuation pathways, but now triggered by a discontinuous change in r. In contrast, 'nematic genesis' polydomains do not show macroscopic soft elasticity [26, 28], and are unsuitable for this experiment.

Soft-mode Ballooning. – Upon cooling a (hypothetical) perfectly-isotropic LCE monodomain, any nematic director $\boldsymbol{n}_0$ could be chosen, and each possibility produces a different but equivalent spontaneous deformation $\boldsymbol{F_s} = \boldsymbol{l}_0^{1/2}$. This broken-symmetery endows cold LCEs with Goldsone-like soft modes of deformation which map the LCE between different but equivalent ground states, accompanied by rotation of the alignment to a new director $\boldsymbol{n}$. Indeed, if we substitute $\boldsymbol{F} \to \boldsymbol{F}\boldsymbol{l}_0^{1/2}$ into eqn. 6 (so that $\boldsymbol{F}$ is now the deformation of the aligned nematic LCE with $\boldsymbol{n}_0$) the elastic energy becomes [5]

$$W_s(\mathbf{F}, \boldsymbol{n}) = \tfrac{1}{2}\mu \mathrm{Tr}(\boldsymbol{l}_0.\boldsymbol{F}^T.\boldsymbol{l}^{-1}.\boldsymbol{F}), \tag{8}$$

where the current director $\boldsymbol{n}$ is now understood as free to rotate within the LCE. This energy is minimised by any distortion in which the director rotates to $\boldsymbol{n}$ and the elastomer undergoes the Goldstone deformation $\boldsymbol{F}_{soft} = \boldsymbol{l}^{1/2}\boldsymbol{R}\boldsymbol{l}_0^{-1/2}$, with $\boldsymbol{R}$ a rotation. Most familiarly, stretch perpendicular to $\boldsymbol{n}_0$ can be accommodated softly (up to $\sqrt{r}$) via reorientation [5, 14], as sketched in Fig. 1(b)i.

Similarly, upon cooling an isotropic LCE balloon at zero pressure, any direction could be chosen for $\boldsymbol{n}_0$, and different choices give different spontaneous deformations, with different volume strains. As previously, an azimuthal director produces a spontaneous dilation $v_s = \sqrt{r}$. In contrast, longitudinal $\boldsymbol{n}_0$ would give $L \to r^{1/3}L$ and $R \to r^{-1/6}R$ with no overall volume strain; homeotropic (radial) director would give $R \to r^{-1/6}R$ and $L \to r^{-1/6}L$ for an overall contraction $v_s = 1/\sqrt{r}$; and oblique director $\boldsymbol{n}_0$ would interpolate these three limits. If one inflates an initially homeotropic balloon, it will traverse these states via director rotation (at zero pressure) until it reaches the azimuthal state, which encloses the largest volume. We thus encounter a "soft" zero-pressure dilation up to $v = r$ (relative to the homeotropic initial state) followed by conventional inflation of the azimuthal balloon until the classical ballooning threshold is reached at $v = v_0^- r$. Similarly, a longitudinal balloon will inflate softly to $v = \sqrt{r}$, then inflate with $\boldsymbol{n}$ azimuthal until ballooning at $v = v_0^- \sqrt{r}$.

However, although monodomain LCEs do deform very softly via director rotation, the stress is never quite zero, and they do return to their original configuration on release. The origin of this non-ideal ("semi-soft") behaviour is the alignment required during monodomain fabrication, which imprints a preferred director orientation and breaks the degeneracy. This behaviour is captured by a"semi-soft" addition to the nematic energy that encodes a preference for the current director $\boldsymbol{n}$ to align with the imprinted director $\boldsymbol{n}_0$ via a non-ideality parameter α:

$$W(\boldsymbol{F}, \boldsymbol{n}) = W_s(\boldsymbol{F}, \boldsymbol{n}) + \tfrac{1}{2}\mu\alpha \mathrm{Tr}\left((\boldsymbol{\delta} - \boldsymbol{n}_0\boldsymbol{n}_0).\boldsymbol{F}^T.(\boldsymbol{n}\boldsymbol{n}).\mathbf{F}\right).$$

This addition can be justified microscopically [29] or phenomenologically [30], and provides an excellent description of director rotation in LCE strips [14]. In particular, in the iconic perpendicular stretch experiment (Fig. 1(b)i), director rotation is delayed until a threshold stretch $\lambda_i = ((r-1)/(r-1-\alpha r))^{1/3}$, then proceeds continuously with increasing stress/stretch (leading to characteristic stress plateau) before completing at $\lambda_f = \sqrt{r}\lambda_i$ [5].

Homeotropic initial alignment. In LCE balloons, non-ideality is essential to resolve the $p - v$ curve during rotation, and probe stability. We start by considering a balloon (R, L, H) with homeotropic initial director, $\boldsymbol{n}_0 = \hat{\boldsymbol{\rho}}$, being inflated by v. Prior to rotation, ($\boldsymbol{n} = \boldsymbol{n}_0$), the semi-soft energy reproduces the neo-Hookean energy and pres-

sure, $w_0(v)$ and $p_0(v)$, with a minimum at $v = 1$ and classical balloon instability at v_0^-. However, past threshold, we expect director rotation towards dominating azimuthal stress, $\boldsymbol{n}_\phi = \sin(\phi)\hat{\boldsymbol{\theta}} + \cos(\phi)\hat{\boldsymbol{\rho}}$. As seen in stretching (Fig. 1(b)i, [5,14]), during rotation, we must allow sympathetic shears, $F_{\theta\rho} = s$ so the LCE can access soft Goldstone-type deformations:

$$\mathbf{F} = \begin{pmatrix} \lambda & 0 & 0 \\ 0 & \eta & s \\ 0 & 0 & 1/(\lambda\eta) \end{pmatrix}. \tag{9}$$

Shear $F_{\rho\theta}$ could also enable soft deformations, but it makes non-circular cross-sections, and (as λ_{zx} in stretched strips [5]) is suppressed (via torques) by azimuthal stress.

Once rotation is complete ($\boldsymbol{n}_{\pi/2} = \hat{\boldsymbol{\theta}}$) the shear must vanish (on symmetry grounds) and the semi-soft energy reduces to $w_{\pi/2} = \mu\pi RHL\left(\eta^2/r + \lambda^2 + r/(\eta^2\lambda^2) + \alpha\eta^2\right)$. During this final portion of inflation we can simply substitute $\lambda = v/\eta^2$ and minimise over η to obtain the energy (and hence the pressure) as a function of v. This again reveals a re-scaled version of a neo-Hookean balloon:

$$w_{\pi/2}(v) = (1+\alpha r)^{1/3} w_0\left(v/v_{\pi/2}\right) \tag{10}$$

$$p_{\pi/2}(v) = (1+\alpha r)^{1/3} p_0\left(v/v_{\pi/2}\right)/v_{\pi/2} \tag{11}$$

where $v_{\pi/2} = r/\sqrt{\alpha r + 1} > 1$ is the minimum of the azimuthal energy, which, reassuringly, reduces to $v_{\pi/2} = r$ in the ideal case, reflecting the ideal end of soft inflation.

To find the energy and pressure during rotation, we substitute our general $\boldsymbol{F}$ and an oblique director $\boldsymbol{n}_\phi$ into the semi-soft energy. We then further substitute $\lambda = v/\eta^2$ and minimise over s, ϕ and η (detailed algebra in SI) to get

$$s = \frac{\eta(r-1)\sin\phi\cos\phi}{v\left(\sin^2\phi + r\left(1-\sin^2\phi\right)\right)}$$

$$\sin^2\phi = \frac{r(v-v_i)}{(r-1)v}, \quad \eta = \left(\frac{2v^4}{v^2 + 2vv_i^{-1} - v^2v_i^{-2}}\right)^{1/6}$$

where $v_i \equiv \sqrt{\frac{r-1}{r-1-\alpha r}}$. As plotted in Fig.5a, director rotation (and sympathetic shear) proceeds between v_i and $v_f = r\,v_i$, again reflecting the ideal degree of soft-inflation.

The balloon director can rotate towards azimuthal in either sense, $\pm\phi$, with opposite shear $\pm s$. Stretched LCE strips famously break into "stripe-domains" of alternate rotation [14], in order to avoid macroscopic shear at the clamps. Initially homeotropic balloons, only shear in the thickness direction, so the displacement is small and unconstrained, leaving no imperative for stripes. Different regions may nevertheless rotate in different senses, leading to domain patterns but not changing the mechanics.

Substituting all these fields back into the full semi-soft energy, we can evaluate to energy and pressure:

$$w_\phi(v) = 3\mu\pi RHL\left(v_i^{-1} - \tfrac{1}{2}vv_i^{-2} + \tfrac{1}{2}v\right)^{2/3} \tag{12}$$

$$p_\phi(v) = \frac{\mu H}{R}\left(v_i^{-1} - \tfrac{1}{2}vv_i^{-2} + \tfrac{1}{2}v\right)^{-1/3}\left(1 - v_i^{-2}\right). \tag{13}$$

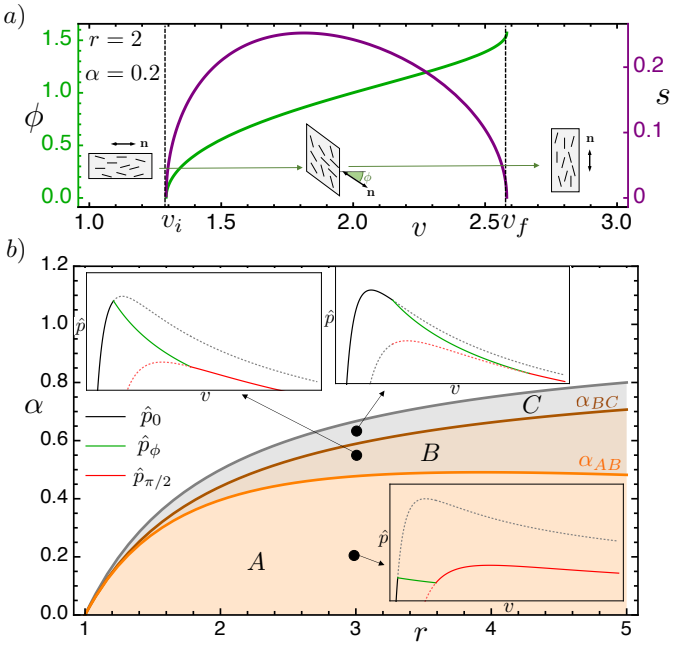

Fig. 5: a) Director rotation angle ϕ (green) and shear s (purple) as a function of v. b) Summary of phase separation behaviour as dependent on α and r. In section A classical and rotational instabilities happen consecutively. In B there is a single instability, started by director reorientation and saturating via the classic instability. In C there is a single instability with classical onset and saturation, but decorated by reorientation. Above the limiting line $\alpha = (r-1)/r$ rotation is suppressed.

Reassuringly, both energy and pressure meet their initial (homeotropic) and final (azimuthal) counterparts continuously at v_i and v_f respectively, leading to continuous $p-v$ curves containing three segments, as shown in Fig.5b. Furthermore, we see that p_ϕ would indeed vanish in the ideal limit $v_i = 1$, and should be strikingly small in real LCEs.

Excitingly, the energy during rotation $w_\phi(v)$ is strictly concave, generating a descending pressure curve, and guaranteeing a sub-critical ballooning during rotation. For an almost ideal LCE ($\alpha \ll 1$, region A of Fig.5b) director rotation starts at very small inflation, $v_i \sim 1$, and immediately nucleates a sub-critical ballooning from homeotropic to azimuthal (via phase-separation under volume control, or a volume jump under pressure control). This initial ballooning is entirely LCE in character, and covers a volume strain $v \sim r$. Additional inflation then occurs with azimuthal director, and the classical ballooning instability occurs later, when $v^- = v_0^-\,v_{\pi/2}$ is reached in the azimuthal energy. If α is larger (region B) the onset of rotation is delayed, and the end of rotation joins $p_{\pi/2}$ after the classical ballooning instability, giving a single combined instability nucleated by director rotation, but saturated classically in the azimuthal state by unwinding polymers. Yet larger α (C) delays rotation beyond the classical ballooning threshold in the homeotropic state, so ballooning starts and finishes classically, but is decorated by director

rotation. The lines between these regions can be found by setting $v_f = v^-_{\pi/2}$ and $v_i = v^-_0$ respectively, to get

$$\alpha_{AB} = \frac{\left(3+\sqrt{21}\right)(r-1)}{r\left(r+\sqrt{21}+3\right)}, \quad \alpha_{BC} = \frac{\sqrt{21}-9}{5}\left(\frac{1-r}{r}\right).$$

Longitudinal initial alignment. Finally, we present the results for a balloon with initially longitudinal director, $\boldsymbol{n}_0 = \hat{\mathbf{z}}$. Following the same steps as before (algebra in SI), the initial (unrotated) energy and pressure are still $w_0(v)$ and $p_0(v)$. Similarly, their fully rotated (azimuthal) counterparts are still $w_{\pi/2}$ and $p_{\pi/2}$ from eqn. (11), but with minimising volume strain $v_{\pi/2} = \sqrt{r/(1+\alpha r)}$, which now recalls the extent of the soft-inflation for an ideal longitudinal balloon, $v = \sqrt{r}$. Between, we expect an oblique rotating director, $\boldsymbol{n}_\phi = \sin\phi\hat{\theta} + \cos\phi\hat{z}$, which demands inclusion of a sympathetic shear $s = F_{\theta z}$. This shear is in-plane (like stretched strips) leading to macroscopic displacements that cause the balloon to twist along its length. Again their are two senses for rotation and shear, and striping may be encountered to eliminate this macroscopic twist (if the ends of the balloon are constrained) but without changing the $p-v$ mechanics.

Going through the same minimizations (s, ϕ and η) we obtain the energy and pressure during rotation:

$$w_\phi(v) = \tfrac{3}{2}\mu\pi RHL\left(2v^2\left(1-v_i^{-4}\right)+4v_i^{-2}+4\right)^{1/3} \quad (14)$$

$$p_\phi(v) = \frac{\mu H}{R}\frac{2v\left(1-v_i^{-4}\right)}{\left(2v^2\left(1-v_i^{-4}\right)+4v_i^{-2}+4\right)^{2/3}} \quad (15)$$

where $v_i = \sqrt{\frac{1-r}{2\alpha r-r+1}}$ and $v_f = \sqrt{\frac{(1-r)r}{r(\alpha r+\alpha-1)+1}}$ denote the start and end of rotation. In this case, the pressure during rotation rises up to a maximum at $v_c = \sqrt{6/\left(1-v_i^{-2}\right)}$ before decreasing, indicating that director rotation can occur continuously up to v_c, and sub-critically thereafter.

We may again construct 3-section pressure curves to examine the stability of longitudinal systems. In the case of small α, Figure 6b, we find the energy remains convex throughout rotation, and ballooning only occurs at the classical ballooning threshold in the fully rotated (azimuthal) state. Upon ballooning (under volume control) phase separation will saturate into v_b (with azimuthal director) and v_a, which may be azimuthal, rotating or longitudinal depending on the Maxwell pressure, which is in turn determined by J_m. However, for sufficiently small α, v_b will surely also be azimuthal, so continuous director rotation will entirely precede azimuthal ballooning. On the other hand, at large α, Figure 6a, the pressure curve of the rotating section has a maximum at v_c, corresponding to an instability. In this case, phase separation will be initiated when the director is partially rotated, and the two phases are guaranteed to have different orientations. The transition between these regimes occurs at:

$$\alpha = \frac{3\left(\sqrt{21}-1\right)(r-1)}{r\left(20r+3\sqrt{21}-3\right)} \quad (16)$$

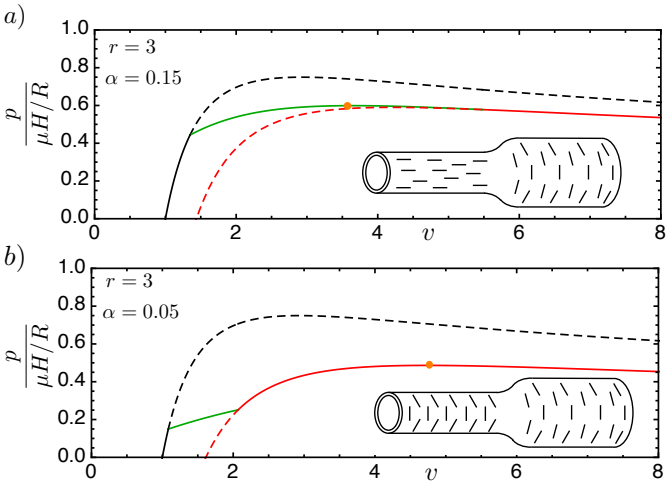

Fig. 6: Pressure curve for initially longitudinal alignment of the director-field. In the case of large α (a) instability is triggered during director rotation, and phase separation is between regions of different alignment. Small α (b) leads to rotation concluding prior to instability, so phase-separation happens entirely within the azimuthal section of the pressure curve.

Discussion. – Ballooning is the original large strain elastic instability. However, in recent years, many more examples have been documented: cavitation, wrinkling, buckling, fingering creasing and beading to name but a few. These instabilities are of considerable interest in soft solids, as they can be used to reversibly sculpt shape. Here we have demonstrated two ways in which the ballooning instability can be controlled and enriched by using LCEs. Firstly, we have seen how the thermal strains of an LCE can trigger ballooning. This process leverages LCEs to create balloons that respond to heat and light. However, it also leaverages ballooning to greatly magnifying the LCEs intrinsic actuation, and generate an explosive sub-critical response that could be used for switching, jumping or threshold-sensing. Such sensors are not limited to the temperature and inflation stimuli considered here, as LCEs can also actuate in response to illumination, electric fields, and swelling with (isotropic or nematic) solvents [5], while inflation can be coupled to many other chemical stimuli via osmosis [11]. Secondly, we have seen how the soft-modes associated with director-rotation within an LCE can produce entirely new modes of ballooning. We anticipate that LCEs, and other soft actuators, can similarly control and enrich a wide range of classical instabilities, facilitating their deployment in shape-shifting devices.

REFERENCES

[1] Mallock A., *Proceedings of the Royal Society of London*, **49** (1891) 458.

[2] Chater E. and Hutchinson J. W., *Journal of Applied Mechanics*, **51** (1984) 269.

[3] Gent A., *International Journal of Non-Linear Mechanics*, **40** (2005) 165.

[4] Meng F., Chen J. Z., Doi M. and Ouyang Z., *AIChE Journal*, **60** (2014) 1393.

[5] Warner M. and Terentjev E. M., *Liquid crystal elastomers* Vol. 120 (Oxford university press) 2007.

[6] De Gennes P.-G. and Prost J., *The physics of liquid crystals* Vol. 83 (Oxford university press) 1993.

[7] Küpfer J. and Finkelmann H., *Die Makromolekulare Chemie, Rapid Communications*, **12** (1991) 717.

[8] De Gennes P.-G., Hébert M. and Kant R., *Artificial muscles based on nematic gels* in proc. of *Macromolecular Symposia* Vol. 113 (Wiley Online Library) 1997 pp. 39–49.

[9] Thomsen D. L., Keller P., Naciri J., Pink R., Jeon H., Shenoy D. and Ratna B. R., *Macromolecules*, **34** (2001) 5868.

[10] Schüring H., Stannarius R., Tolksdorf C. and Zentel R., *Macromolecules*, **34** (2001) 3962. https://doi.org/10.1021/ma000841q

[11] Jampani V., Volpe R., de Sousa K. R., Machado J. F., Yakacki C. and Lagerwall J., *Science advances*, **5** (2019) eaaw2476.

[12] Golubović L. and Lubensky T., *Physical review letters*, **63** (1989) 1082.

[13] Olmsted P. D., *Journal de Physique II*, **4** (1994) 2215.

[14] Finkelmann H., Kundler I., Terentjev E. and Warner M., *Journal de Physique II*, **7** (1997) 1059.

[15] DeSimone A. and Dolzmann G., *Archive for rational mechanics and analysis*, **161** (2002) 181.

[16] Wang M. C. and Guth E., *The Journal of Chemical Physics*, **20** (1952) 1144.

[17] Giudici A. and Biggins J. S., *arXiv preprint arXiv:2005.10535*, (2020) .

[18] Gent A. N., *Rubber chemistry and technology*, **69** (1996) 59.

[19] Kaufhold W., Finkelmann H. and Brand H. R., *Die Makromolekulare Chemie: Macromolecular Chemistry and Physics*, **192** (1991) 2555.

[20] Mistry D., Connell S. D., Mickthwaite S., Morgan P. B., Clamp J. H. and Gleeson H. F., *Nature communications*, **9** (2018) 1.

[21] Rodriguez E. K., Hoger A. and McCulloch A. D., *Journal of biomechanics*, **27** (1994) 455.

[22] Broer D. J., *Molecular Crystals and Liquid Crystals Science and Technology. Section A. Molecular Crystals and Liquid Crystals*, **261** (1995) 513.

[23] Ware T. H., McConney M. E., Wie J. J., Tondiglia V. P. and White T. J., *Science*, **347** (2015) 982.

[24] Rudykh S., Bhattacharya K. and deBotton G., *International Journal of Non-Linear Mechanics*, **47** (2012) 206.

[25] Li T., Keplinger C., Baumgartner R., Bauer S., Yang W. and Suo Z., *Journal of the Mechanics and Physics of Solids*, **61** (2013) 611.

[26] Urayama K., Kohmon E., Kojima M. and Takigawa T., *Macromolecules*, **42** (2009) 4084.

[27] Biggins J., Warner M. and Bhattacharya K., *Physical review letters*, **103** (2009) 037802.

[28] Biggins J., Warner M. and Bhattacharya K., *Journal of the Mechanics and Physics of Solids*, **60** (2012) 573.

[29] Verwey G. and Warner M., *Macromolecules*, **30** (1997) 4189.

[30] Biggins J., Terentjev E. and Warner M., *Physical Review E*, **78** (2008) 041704.

SUPPLEMENTARY INFORMATION

Semi-soft energy. – We consider a cylindrical LCE balloon in $(\hat{\boldsymbol{z}}, \hat{\boldsymbol{\theta}}, \hat{\boldsymbol{\rho}})$ cylindrical coordinates. As in the main text, the balloon is fabricated with length L, radius R and thickness H and initial director $\boldsymbol{n}_0$. It then undergoes a deformation $\boldsymbol{F}$ leading to a final director $\boldsymbol{n}$. The balloon's semi-soft elastic energy is:

$$\frac{w}{\mu\pi RHL} = \mathrm{Tr}(\boldsymbol{l}_0.\boldsymbol{F}^T.\boldsymbol{l}^{-1}.\boldsymbol{F}) + \alpha\mathrm{Tr}((\boldsymbol{\delta} - \boldsymbol{n}_0\boldsymbol{n}_0).\boldsymbol{F}^T.(\boldsymbol{n}\boldsymbol{n}).\boldsymbol{F}), \tag{17}$$

where the step-length tensor $\boldsymbol{l} = r^{-1/3}\left(\boldsymbol{\delta} + (r-1)\boldsymbol{n}\boldsymbol{n}\right)$.

Radial homeotropic. – We first consider a balloon with radial initial director, $\boldsymbol{n}_0 = \hat{\boldsymbol{\rho}}$, and hence $\boldsymbol{l}_0 = \mathrm{diag}(r^{-1/3}, r^{-1/3}, r^{2/3})$. If, during inflation, the director rotates to an angle ϕ in the $\rho-\theta$ plane, $\boldsymbol{n}_\phi = \sin(\phi)\hat{\boldsymbol{\theta}} + \cos(\phi)\hat{\boldsymbol{\rho}}$, the step-length tensor is:

$$\boldsymbol{l}_\phi = r^{-1/3}\begin{pmatrix} 1 & 0 & 0 \\ 0 & r\sin^2(\phi) + \cos^2(\phi) & (r-1)\sin(\phi)\cos(\phi) \\ 0 & (r-1)\sin(\phi)\cos(\phi) & r\cos^2(\phi) + \sin^2(\phi) \end{pmatrix}. \tag{18}$$

Note that this simplifies to $\boldsymbol{l}_{\pi/2} = \mathrm{diag}(r^{-1/3}, r^{2/3}, r^{-1/3})$ for the fully rotated, $\phi = \pi/2$ director. Substituting $\boldsymbol{l}_0$, $\boldsymbol{n}_0$, $\boldsymbol{l} = \boldsymbol{l}_\phi$ into the energy, along with $\boldsymbol{F}$ appearing in equation (9) in the main text, and then introducing the volume strain measure via $\lambda = v/\eta^2$, we obtain the total energy:

$$\begin{aligned}\frac{w}{\mu\pi RHL} =& \frac{\eta^2}{r}\left(r\cos^2\phi + \sin^2\phi\right) + s\left(s\left(r\cos^2\phi + \sin^2\phi\right) - \frac{\eta(r-1)\sin\phi\cos\phi}{v}\right) \\ &+ \frac{\eta}{v}\left(\frac{\eta\left(r\sin^2\phi + \cos^2\phi\right)}{v} - (r-1)s\sin\phi\cos\phi\right)v + \frac{v^2}{\eta^4} + \alpha\eta^2\sin^2\phi.\end{aligned} \tag{19}$$

For the unrotated director ($\phi = 0$), the free energy simplifies to the neo-Hookean elastic energy, $w_0 = \mu\pi RHL\left(\eta^{-2}\lambda^{-2} + \eta^2 + \lambda^2\right)$ which can be trivially expressed as a function of v to obtain $w_0(v)$ as in eqn (2) in the main text. Similarly, the rotated section ($\phi = \pi/2$) reads $w_{\pi/2} = \mu\pi RHL\left(\eta^2/r + \lambda^2 + r/(\eta^2\lambda^2) + \alpha\eta^2\right)$ leading to $w_{\pi/2}(v) = (1+\alpha r)^{1/3} w_0\left(v/v_{\pi/2}\right)$.

To find the energy $w(v)$ during rotation, we start by minimising the shear s, setting $\frac{\partial w_\phi}{\partial s} = 0$. This is a linear equation yielding

$$s = \frac{\eta(r-1)\sin\phi\cos\phi}{v\left(\sin^2\phi + r\left(1 - \sin^2\phi\right)\right)}. \tag{20}$$

Substituting this shear back in the energy we find:

$$\frac{w_\phi}{\mu\pi RHL} = \frac{\eta^2((\alpha-1)kr + k + r)}{r} - \frac{\eta^2 r}{v^2(k(r-1) - r)} + \frac{v^2}{\eta^4}, \tag{21}$$

where $k = \sin^2\phi$. We can now minimise with respect to both k and η simultaneously to obtain:

$$k = \frac{r(v - v_i)}{(r-1)v} \tag{22}$$

$$\eta = \left(\frac{rv^4(k(r-1) - r)}{v^2(k(r-1) - r)((\alpha-1)kr + k + r) - r^2}\right)^{1/6} = \left(\frac{2v^4}{v^2 + 2vv_i^{-1} - v^2v_i^{-2}}\right)^{1/6} \tag{23}$$

where $v_i = \sqrt{\frac{r-1}{r-1-\alpha r}}$. Substituting all the minimised fields back in eqn. (21) one obtains eqns. (12) and (13) in the main text.

Longitudinal Director. – For the longitudinal initial director, we set $\boldsymbol{n}_0 = \hat{\boldsymbol{z}}$ and, since rotation and shear happens now in the $z-\theta$ plane, we must again allow for sympathetic shears, $F_{\theta z} = s$ so the LCE can access soft Goldstone-type deformations, so that

$$\boldsymbol{F} = \begin{pmatrix} \lambda & 0 & 0 \\ s & \eta & 0 \\ 0 & 0 & \xi \end{pmatrix}. \tag{24}$$

The $F_{z\theta}$ component could also enable soft deformations, but it breaks the rotational symmetry and (as λ_{zx} in stretched strips [5]) is suppressed (via torques) by azimuthal stress. We also have $\boldsymbol{l}_0 = \mathrm{diag}(r^{2/3}, r^{-1/3}, r^{-1/3})$ and the general step-length tensor, corresponding to the director $\boldsymbol{n}_\phi = \cos\phi\hat{\boldsymbol{z}} + \sin\phi\hat{\boldsymbol{\theta}}$, is given by:

$$\boldsymbol{l}_\phi = r^{-1/3}\begin{pmatrix} r\cos^2\phi + \sin^2\phi & (r-1)\sin\phi\cos\phi & 0 \\ (r-1)\sin\phi\cos\phi & r\sin^2\phi + \cos^2\phi & 0 \\ 0 & 0 & 1 \end{pmatrix}. \tag{25}$$

We can substitute each term in the trace formula, equation (17), and obtain the free energy:

$$\begin{aligned}\frac{w_\phi}{\mu\pi RHL} =& \eta^2\left(\frac{\sin^2(\phi)}{r} + \cos^2(\phi)\right) + s\left(rs\left(\frac{\sin^2(\phi)}{r} + \cos^2(\phi)\right) + \frac{(1-r)v\sin(\phi)\cos(\phi)}{\eta^2}\right) \\ &+ \frac{v}{\eta^2}\left((1-r)s\sin(\phi)\cos(\phi) + \frac{rv}{\eta^2}\left(\frac{\cos^2(\phi)}{r} + \sin^2(\phi)\right)\right) + \frac{\eta^2}{v^2} + \alpha\eta^2\sin^2(\phi)\end{aligned}$$

Again, we first minimise with respect to the shear s, so that

$$s = \frac{(r-1)v\sin(\phi)\cos(\phi)}{\eta^2\left(\sin^2(\phi) + r\cos^2(\phi)\right)}. \tag{26}$$

We substitute the minimised shear back in the energy and obtain

$$\frac{w_\phi}{\mu\pi RHL} = \frac{\eta^2 k}{r} - \frac{rv^2}{\eta^4(k(r-1)-r)} + \eta^2\left((\alpha-1)k + \frac{1}{v^2} + 1\right) \tag{27}$$

where we still have that $k = \sin^2\phi$. Minimising both k and η leads to:

$$k = \frac{2r(v-v_i)(v+v_i)}{(r-1)v^2\left(v_i^2+1\right)}, \quad \eta = \left(\frac{2v^4\left(v_i^6+v_i^4\right)}{\left(\left(v_i^2-1\right)v_i + 2v_i^3v^{-2}\right)^2}\right)^{1/6}. \tag{28}$$

Finally, substituting all the fields back in eqn. (27) we obtain eqns. (14) and (15) from the main text.